



Woody plant cover estimation in drylands from Earth Observation based seasonal metrics

Brandt, Martin Stefan; Hiernaux, Pierre; Tagesson, Håkan Torbern; Verger, Alexandre; Rasmussen, Kjeld; Diouf, Abdoul Aziz; Mbow, Cheikh; Mougin, Eric; Fensholt, Rasmus

Published in:
Remote Sensing of Environment

DOI:
[10.1016/j.rse.2015.10.036](https://doi.org/10.1016/j.rse.2015.10.036)

Publication date:
2016

Document version
Peer reviewed version

Citation for published version (APA):
Brandt, M. S., Hiernaux, P., Tagesson, H. T., Verger, A., Rasmussen, K., Diouf, A. A., ... Fensholt, R. (2016). Woody plant cover estimation in drylands from Earth Observation based seasonal metrics. *Remote Sensing of Environment*, 172, 28-38. <https://doi.org/10.1016/j.rse.2015.10.036>

1 **Title:**

2 **Woody plant cover estimation in drylands from Earth Observation based seasonal metrics**

3

4 **Authors:**

5 Martin Brandt¹, Pierre Hiernaux², Torbern Tagesson¹, Aleixandre Verger³, Kjeld Rasmussen¹, Abdoul Aziz

6 Diouf⁴, Cheikh Mbow⁵, Eric Mougin², Rasmus Fensholt¹

7

8

9 ¹Department of Geosciences and Natural Resource Management, University of Copenhagen, 1350

10 Copenhagen, Denmark; martin.brandt@mailbox.org

11 ² Geosciences Environnement Toulouse (GET), Observatoire Midi-Pyrénées, UMR 5563

12 (CNRS/UPS/IRD/CNES), 14 Avenue Edouard Belin, 31400 Toulouse, France;

13 pierre.hiernaux@wanadoo.fr

14 ³ CREAM, Cerdanyola del Vallès, 08193, Catalonia, Spain; verger@creaf.uab.cat.

15 ⁴ Centre de Suivi Ecologique, BP 15532 Dakar-Fann, Senegal; dioufee@gmail.com.

16 ⁵ Science Domain 6, ICRAF (World Agroforestry Center), 00100 Nairobi, Kenya; c.mbow@cgiar.org.

17

18

19 **Corresponding author:**

20 Martin Brandt

21 Östervoldgade 10

22 1350 Copenhagen, Denmark

23 martin.brandt@mailbox.org

24

25

26

27 **Abstract**

28

29 From *in situ* measured woody cover we develop a phenology driven model to estimate the canopy cover of
30 woody species in the Sahelian drylands at 1 km scale. The model estimates the total canopy cover of all
31 woody phanerophytes and the concept is based on the significant difference in phenophases of dryland trees,
32 shrubs and bushes as compared to that of the herbaceous plants. Whereas annual herbaceous plants are only
33 green during the rainy season and senescence occurs shortly after flowering towards the last rains, most
34 woody plants remain photosynthetically active over large parts of the year. We use Moderate Resolution
35 Imaging Spectroradiometer (MODIS) and Satellite pour l'Observation de la Terre (SPOT) - VEGETATION
36 (VGT) Fraction of Absorbed Photosynthetically Active Radiation (FAPAR) time series and test 10 metrics
37 representing the annual FAPAR dynamics for their ability to reproduce *in situ* woody cover at 43 sites (163
38 observations between 1993 and 2013) in the Sahel. Both multi-year field data and satellite metrics are
39 averaged to produce a steady map. Multiple regression models using the integral of FAPAR from the onset of
40 the dry season to the onset of the rainy season, the start date of the growing season and the rate of decrease
41 of the FAPAR curve achieve a cross validated r^2 /RMSE (in % woody cover) of 0.73/3.0 (MODIS) and
42 0.70/3.2 (VGT). The extrapolation to Sahel scale shows agreement between VGT and MODIS at an almost
43 nine times higher woody cover than in the global tree cover product MOD44B which only captures trees of a
44 certain minimum size. The derived woody cover map of the Sahel is made publicly available and represents
45 an improvement of existing products and a contribution for future studies of drylands quantifying carbon
46 stocks, climate change assessment, as well as parametrization of vegetation dynamic models.

47

48

49 **Keywords:** woody cover, phenology, FAPAR, drylands, Sahel, MODIS, VEGETATION, multilinear model

50 **Introduction**

51

52 Trees, shrubs and bushes are an important element of savanna ecosystems and for livelihoods in dryland
53 areas dependent on fuel-wood supply. During the past decades, several studies have seriously questioned
54 prevailing narratives of a widespread and Sahel-wide decrease in woody cover (Spiekermann et al., 2015;
55 Rasmussen et al., 2006; Rasmussen et al., 2001), commending the relevance of large scale woody cover
56 monitoring systems.

57 Most studies estimating tree canopy cover with remote sensing rely on high resolution imagery which
58 allow direct mapping at a scale recognizing trees of a certain size as objects (e.g. Karlson et al., 2014;
59 Sterling and Orr, 2014; Herrmann et al., 2013; San Emeterio and Mering, 2012; Rasmussen et al., 2011).
60 However, imageries with a spatial resolution of 1-5 m are cumbersome to process, expensive, susceptible to
61 clouds, and do only provide a static situation for a limited spatial area. Moreover, considering trees as
62 objects, smaller isolated woody plant are missed and individual woody plants are hard to separate in dense
63 thickets (Spiekermann et al., 2015). Global tree cover products at 30 m using Landsat (Sexton et al., 2013)
64 and 250 m using Moderate Resolution Imaging Spectroradiometer (MODIS) are trained with higher
65 resolution imagery (Hansen et al., 2003; DeFries et al., 2001) and are available for assessing states of canopy
66 cover and deforestation rates. However, the reliability of these products in semi-arid regions with open tree
67 cover is contested (e.g. Hansen et al., 2005; Herrmann et al., 2013; Gessner et al., 2013) and limited
68 evaluations against ground observations have been done for drylands in general and for the Sahel in
69 particular.

70 The leafing of trees and shrubs in semi-arid areas like the Sahel is not temporally uniform. This suggests
71 that large scale woody cover modeling from moderate to coarse spatial resolution Earth Observation (EO)
72 data can potentially be improved by including vegetation metrics covering various stages of the growing
73 season cycle, and not only images or variables representing snapshots in time. This is particularly important
74 in the Sahelian zone, where the vegetation is characterized by a rapid phenological cycle driven by the short
75 rainy season where most of the observations in the optical domain are missing or affected by noise due to
76 cloud cover. The spatial resolution of MODIS (250-1000 m) and Satellite Pour l'Observation de la Terre,
77 (SPOT) - Vegetation (VGT) (1000 m) is traditionally considered a limitation for vegetation monitoring,

78 however, major morphological units, widespread deforestation and regional climate dynamics are visible at
79 this scale and represent the spatial characteristics of the Sahel area (Vintrou et al., 2014). Given the high
80 temporal sampling frequency of MODIS and VGT, noise from cloud cover can be suppressed and various
81 seasonal metrics related to phenology of the green vegetation mixed in a pixel can be derived (Horion et al.,
82 2014). Recent studies show that the dominant woody species in the Sahel have a significant footprint in long-
83 term trends of coarse satellite data time series (Brandt et al., 2015), but it remains unclear how woody cover
84 affects the annual vegetation curve as measured by EO data.

85 We suggest an approach driven by vegetation phenology including *in situ* measured woody cover data
86 across the Sahel and seasonal metrics from time series of MODIS and SPOT-VGT. The method is an indirect
87 estimation of the canopy cover of all woody phanerophytes including trees, shrubs and bushes (thus the
88 expression woody cover is used), and is based on the significant difference in phenophases of woody plants
89 as compared to that of the herbaceous plants (Horion et al., 2014; Wagenseil and Samimi, 2007; De Bie et
90 al., 1998). In the Sahel, annual herbaceous plants are only green during the rainy season from June to
91 October (depending on the latitudinal position and of the vagaries of annual rain distribution) and senescence
92 occurs after flowering in September towards the last rain events of the season. The leafing of most trees and
93 shrubs is longer (Mbow et al., 2013; De Bie et al., 1998), with several evergreen species, and many woody
94 species green-up ahead of the rains during the last month of the dry season, while annual herbaceous are
95 dependent on the first rains to germinate (Horion et al., 2014; Seghieri et al., 2012; Hiernaux et al., 1994).
96 The Fraction of Absorbed Photosynthetically Active Radiation (FAPAR) quantifies the fraction of the
97 photosynthetic active radiation absorbed by green vegetation (Baret et al, 2013; Myneni and Williams,
98 1994). FAPAR seasonal metrics derived from EO data highlighting the differences in phenology between
99 annual herbaceous and woody plants are considered suitable indicators of photosynthetic activity of woody
100 canopies.

101 Based on the observation that the phenology of woody vegetation in semi-arid areas is distinctive in the
102 dry season, our objectives are (1) to find evidence for the relationship between satellite derived seasonal
103 metrics of FAPAR and *in situ* measured woody cover, (2) to create a woody cover map for the 1999-2013
104 period for the Sahel belt, and (3) to compare the modeled and *in situ* measured woody cover with an existing
105 global tree cover product.

106

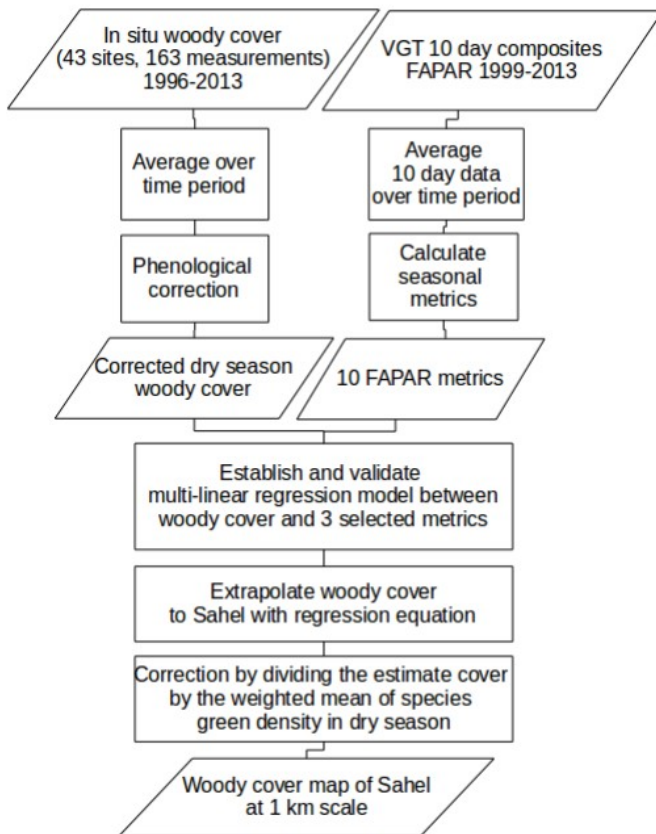
107 **Materials and Methods**

108

109 ***Conceptual approach***

110 The concept of this study is to establish a multi-linear regression between ground based woody cover
111 measurements from Mali and Senegal and satellite derived seasonal metrics from VGT and MODIS time
112 series (Fig. 1). Both field and satellite data are averaged over their period of acquisition to produce a steady
113 map. Based on the assumption that dry season greenness can be used to separate woody from herbaceous
114 production 10 metrics representing the annual FAPAR dynamics are tested to model the total canopy cover
115 of woody plants. The woody canopy cover measured at the field sites is adjusted prior to correlation with
116 satellite data relating to the degree of leaf-out typically occurring in the dry season months. This
117 phenological correction depends on the typical phenological behavior of the component woody species and
118 is thus site specific. To predict the total woody cover at Sahel scale, the correction is based on an estimated
119 mean phenology of all woody plants of the Sahel region.

120

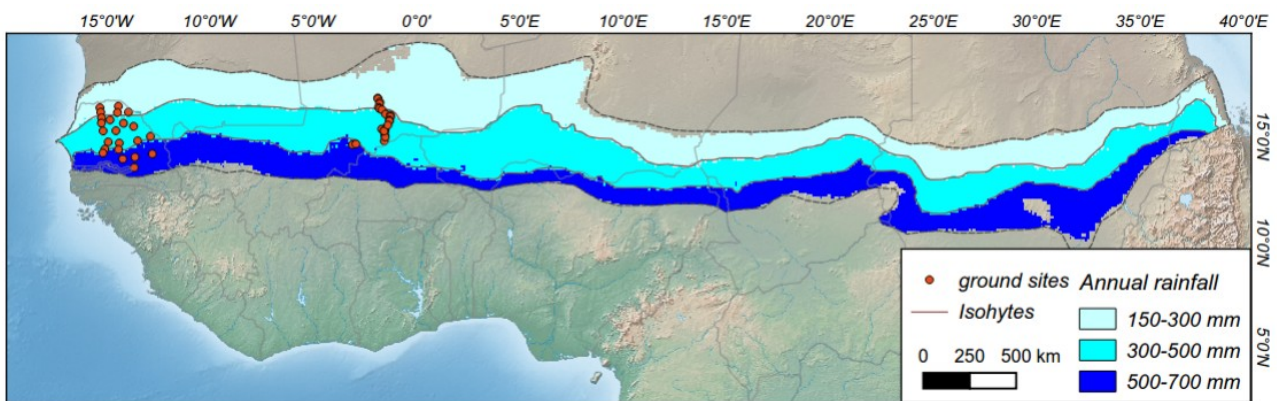


121 *Figure 1: Conceptual approach of this study exemplified for VGT FAPAR*

122 **Study area**

123 The Sahel extends from the Atlantic Ocean in the west to the Red Sea in the east (approximately 6000
 124 km). The bioclimate is considered tropical arid in the north and semi-arid in the south (Sayre et al., 2013; Le
 125 Houérou, 1980). The average annual precipitation varies between 150 mm and 700 mm from north to south.
 126 The delineation (Fig. 2) is derived from African Rainfall Climatology Version 2 (1982–2013) satellite based
 127 rainfall data (Jobard et al., 2011). The rainy season is directly linked to the West African Monsoon with a
 128 length of 1-4 months, an annual peak in precipitation in August (Barbé and Lebel, 1997), and an increasing
 129 rate of annual rainfall along the north-south gradient with approximately 1-2 mm per km (Le Houérou,
 130 1980). The Sahel is subdivided into three biogeographical zones matching the rainfall zones (Fig. 2): the
 131 northern Sahel (Saharo-Sahelian), the central Sahel (Sahelian proper) and the southern Sahel (Sudano-
 132 Sahelian) where rainfed crops largely extend. The northern Sahel is characterized by the abundance of spiny
 133 trees *Acacia* (*Mimosoidae*), *Balanites*, *Ziziphus* and also of *Capparidaceae*. In central Sahel spiny
 134 *Mimosoidae* associate with broadleaf *Combretaceae*, while in southern Sahel woody plants are more diverse
 135 with the association of *Combretaceae* with *Fabaceae* and *Rubiaceae*. Throughout, the herbaceous vegetation

136 is dominated by annual herbaceous, mainly *Gramineae* with C4 photosynthesis type (Hiernaux and Le
137 Houérou, 2006). No significant vegetation gradient is present from west to east and the elevation is generally
138 low. Unique datasets of *in situ* observed woody cover are available for Senegal and the Gourma region, Mali
139 and are distributed over three major rainfall zones (Fig. 2). The study sites cover different ecoregions with
140 sandy and ferruginous soils prevailing. Although there are differences in land-use history between Senegal
141 and Gourma, the two regions share the Sahel monsoonal climate, flora, edaphic traits (range of soil textures,
142 organic and nutrient content) and the pastoral systems, justifying the use of all available ground data for a
143 model being representative at the Sahel scale. The study sites are well described in Diouf et al. (2015),
144 Brandt et al. (2015), Mougín et al., (2009), Hiernaux et al. (2009) and Dardel et al. (2014).
145
146



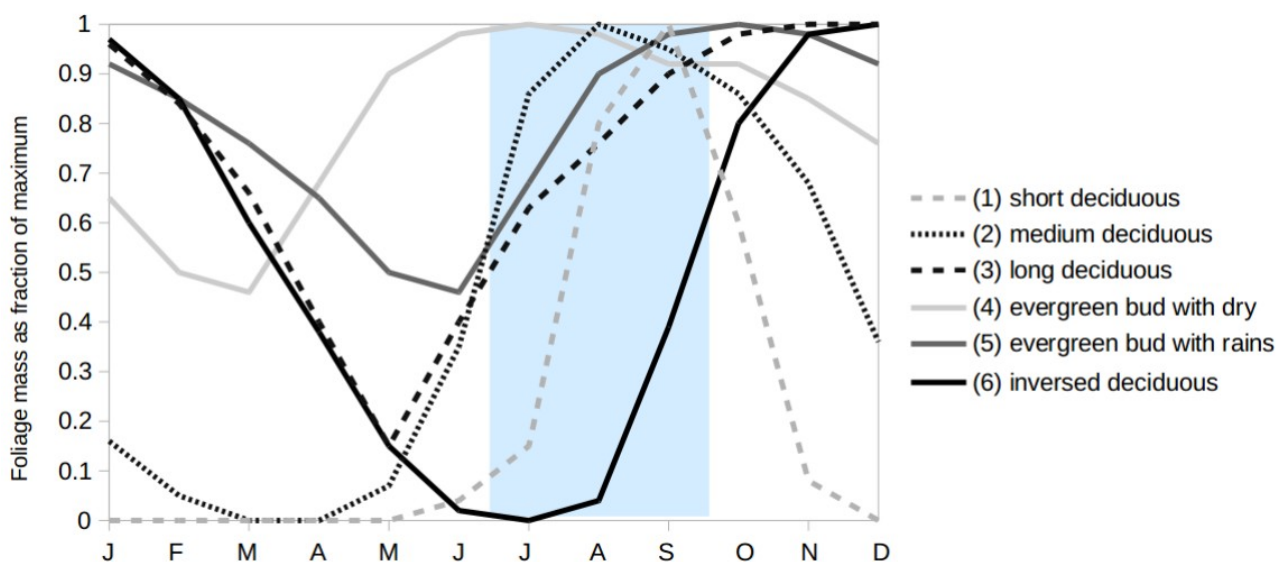
147
148 *Figure 2: Overview of the Sahel zone and location of the 43 ground monitoring sites covering Senegal (west) and the*
149 *Gourma region in Mali. The Sahel delineation is based on annual average precipitation (African Rainfall Climatology*
150 *Version 2 1983–2013).*

151

152 ***Phenological behavior of Sahelian herbaceous and woody vegetation***

153 The herbaceous layer is only short lasting green (less than a 4-month period) in the Sahel (Mougín et al.,
154 2014; Vries, and Djitéye, 1982) causing a strong peak in the seasonality of vegetation during the rainy
155 season. Senescence of the annual herbaceous vegetation shortly after flowering is determined by a biological
156 clock, regardless of eventual late rains (photoperiodicity). The herbaceous vegetation may also die because
157 of lack of soil humidity following a long interruption in rainfall, without succeeding regrowth if later rain

158 occurs. The standing mass of annual herbaceous vegetation is characterized by a very rapid increasing and
 159 decreasing rate, shown e.g. in a herbaceous growth simulation model in Tracol et al. (2006) or Leaf Area
 160 Index (LAI) measurements in Mougin et al. (2014). The recurrent vegetation wilt and die from early
 161 September to late October, and remains photosynthetically inactive until the new germination with the onset
 162 of the following rainy season. For woody vegetation, six different types of phenological behavior are
 163 characterized in Hiernaux et al., (1994) (Fig. 3): (1) short deciduous with species shedding their leaves at the
 164 onset of the dry season (*Commiphora africana*, *Euphorbia balsamifera*, *Acacia seyal*), (2) at the end of the
 165 year (*Combretum micranthum*, *Acacia senegal*, *Pterocarpus lucens*) (3) semi-deciduous (e.g. *Acacia*
 166 *raddiana*, *Guiera senegalensis*), (4+5) two types of evergreens depending on the period of leaf renewal,
 167 either at the onset of the wet season (*Balanites aegyptiaca*, *Combretum glutinosum*), or the onset of the dry
 168 season (*Boscia senegalensis*, *Maerua crassifolia*), and (6) a particular case for *Faidherbia albida* shedding
 169 leaves during the rainy season. For more details and species lists see De Bie et al., (1998), Seghieri et al.,
 170 (2012) and Hiernaux et al., (1994). Despite these differences and short deciduous species shedding their
 171 leaves early in the dry season, it is hypothesized that the signal from the photosynthetically active woody
 172 plants during the long lasting dry season impacts the shape of the FAPAR curve as derived from on
 173 continuously recorded satellite data at a 1 km scale.



174

175 Figure 3: Seasonal distribution of woody leaf mass depending on the phenological type, modeled within the STEP

176 primary production simulation model (Mougin et al., 1995). The months of the wet season during which herbaceous
177 grow are highlighted in a shaded box. Illustrations of typical herbaceous growing curves can be found in Mougin et al.,
178 (2014).

179

180 **Ground based woody cover estimation**

181 The study includes *in situ* measured woody cover (trees and shrubs regardless of size) data of 43
182 monitoring sites; 22 in Senegal and 21 in the Gourma region of Mali. Woody cover in Senegal was measured
183 every two years in the end of the rainy season, from 1998 to 2013, whereas the Gourma measurements
184 consist of data recorded in 1993, 2002 and 2005 (Hiernaux et al., 2009). A method called circular plots
185 census was applied for canopy cover estimation both in Senegal and Mali (Hiernaux et al., 2009). The crown
186 cover was surveyed using a systematic and replicable sampling method. Each monitoring site is a 1x1 km
187 plot selected within a homogeneous area of 3x3 km and was inventoried through four circular plots of up to
188 one hectare by woody plant category (generally trees/shrubs/bushes), separated by a distance of 200 m along
189 a transect line of 1 km. The size of the circular plots depends on the density of the woody population but
190 includes a minimum of 10 individuals per plot. In each plot the species of all individuals of trees and shrubs
191 were recorded and height and basal diameter of crowns were measured. These measures were averaged per
192 plot and per site providing means and standard deviations of tree and shrub canopy cover, and the
193 contribution of each species to the overall cover. More details on the methods are provided in Hiernaux et al.
194 (2009).

195

196

197 **Correcting the relation between *in situ* woody cover and dry season FAPAR**

198 The signal measured by satellite FAPAR proposed to separate the woody signal from the herbaceous
199 vegetation is not canopy cover but green density of the canopy cover during the dry season. This green
200 density from October to June depends on the phenological behavior of woody species as shown in Figure 3.
201 For example, sites dominated by short deciduous *Acacia seyal* have a low dry season FAPAR relative to the
202 canopy cover, while a *Faidherbia albida* dominated stand has the opposite. Thus, the relationship between *in*
203 *situ* measured cover and the dry season FAPAR metrics can be adjusted using the phenological behavior of

204 the woody plants from October to June to derive a corrected woody cover . Leaf seasonality of the six types
205 of phenological behavior has been modeled within the STEP (Sahelian Transpiration, Evaporation, and
206 Productivity) primary production simulation model (Mougin et al., 1995; Tracol et al., 2006) using data
207 derived from monthly monitoring of sampled branchlets (1 cm diameter 3 per woody plants -edge, top and
208 interior of the canopy-, 6 plant per species and site) from Niono (1979-1983) and Gourma sites (1984-1993)
209 (see Hiernaux et al., 1994) with additional data from the Gourma sites between 2005-2010. The monthly
210 distribution of foliage mass expressed as a fraction of the maximum mass is shown in Figure 3 and has been
211 extracted for each of the six foliage phenologies to account for the variable foliage density of woody plant
212 species during the dry season. For each of the 43 ground sites, all sampled species were attributed to one of
213 the six phenological behavior classes and thereby given the mean foliage density from October to June
214 (scFD). Then, at site scale, the foliage density of all canopy cover (tFD) was calculated as the mean scFD of
215 all woody species present at the site weighted by the relative contribution of the species (scWC) to total
216 woody cover of the site (tWC)

217 As an example, a two species site with *C. glutinosum* at 20% from 24% total cover (*tWC*) and a dry season
218 mean foliage density (sdFD) of 0.78 (being evergreen) associated to *Sclerocarya birrea* at 4% canopy cover
219 and a scFD of 0.28 (being medium deciduous), has a site foliage density of canopy cover $tFD = 0.78 (20/24)$
220 $+ 0.28 (4/24) = 0.70$. The site's woody cover was then corrected (*cWC*) by multiplying the *in situ* canopy
221 cover with the site foliage density (tFD).

222

223 ***Satellite products***

224 We used Geoland Version 1 (GEOV1) SPOT VGT and MODIS MOD15A2 FAPAR satellite datasets as a
225 proxy to estimate the photosynthetic plant activity for the periods 1999-2013 (VGT) and 2000-2013
226 (MODIS) (Yang et al., 2006; Fensholt et al., 2004; Baret et al., 2013). We use two different datasets to test
227 the proposed methodology for robustness and data related bias. Both GEOV1 and MODIS products are
228 available at 1 km spatial resolution and were reprojected to a geographical projection system for this study.

229 The GEOV1 Copernicus global land products are derived from SPOT VGT data using a neural-network
230 machine-learning algorithm (Verger et al., 2008). Directionally normalized VGT reflectances (Roujean et al.
231 1992) from the top of the canopy in the red, near-infrared, and short-wave infrared bands derived from the

232 CYCLOPES processing line (Baret et al., 2007) are used as inputs. The neural network was trained with
233 MODIS and CYCLOPES FAPAR data which were fused by assigning more weight to the CYCLOPES
234 products for low FAPAR values and to the MODIS ones for high values (Weiss et al., 2007). The temporal
235 sampling of GEOV1 is 10 day with a 30-day compositing window. Further details for the training of the
236 neural networks and the generation of the GEOV1 product are provided in Baret et al (2013).

237 The MODIS FAPAR product relies on a biome dependent look-up table inversion of a radiative transfer
238 model which ingests red and near infrared bidirectional reflectance factor values, their associated
239 uncertainties, the view-illumination geometry, and biome type (within eight types based on the MOD12Q1
240 land cover map) (Myneni et al., 2002). The MODIS FAPAR product is generated by selecting the maximum
241 FAPAR value in an 8-day compositing period.

242 A global tree cover product based on MODIS (MOD44B) V501 is included for comparison purposes and
243 is supposed to map canopy cover of trees greater than 5 m in height, thus not considering small trees, shrubs
244 and bushes, which are included in our *in situ* data (Townshend et al, 2011; Hansen et al., 2002). MOD44B
245 V501 applies a decision tree using Landsat, Ikonos and field data training sets and is based on previous work
246 by Hansen et al. (2003) and DeFries et al. (2001). It is available at annual basis at a 250 m spatial resolution
247 and we resampled it to 1 km using the nearest neighbor technique to match the spatial resolution of the
248 FAPAR products used. Then the average values over the period 2000-2013 were computed. For the sake of
249 brevity, we do not provide a comparison with the Landsat tree cover continuous field data (Sexton et al.,
250 2013) because it was found to be closely related to MOD44B and it compares in a similar way to our
251 estimates.

252 Polygons were drawn around the homogeneous area (approximately 3 x 3 km) of the ground monitoring
253 sites and all 1 km pixels encompassed by a polygon were averaged for each site. Sites without distinct
254 seasonality (limited EO vegetation seasonality detection ability, next section) were excluded from the
255 analysis, reducing the available Gourma sites from 25 to 21.

256

257

258 ***Extraction of satellite seasonal metrics***

259 Seasonal metrics can be highly dynamic (Broich et al., 2014). In the interest of developing a robust and

260 stable relationship between ground observations and satellite metrics, both ground and satellite data were
261 averaged over the period of acquisition prior to extraction of the pixel values. The original temporal
262 frequency for satellite time series was kept, resulting in 8 day (MODIS) and 10 day (VGT) average data.

263 Timesat was used to derive seasonal parameters from satellite time series (Jönsson & Eklundh, 2004).
264 Timesat has been widely used in the Sahel area to detect seasonal dynamics related to the phenology of
265 vegetation and describing the shape of the annual vegetation curve reflected in satellite data (e.g. Horion et
266 al., 2014; Herrmann et al., 2013; Fensholt et al., 2013). The derived seasonal metrics are summarized in
267 Table 1 and illustrated in Figure 4. The values between the end of the growing season (EOS) and the start of
268 the next growing season (SOS) were integrated to a dry season integral (DSINT) by subtracting the small
269 integral (SINT) from the annual integral. Thus the DSINT also includes the rainy season values below the
270 base level (BASE) (Fig. 4), considering that annual herbaceous spontaneous species are starting from zero
271 green, while woody plants have already put leaves explaining the level of the BASE being above zero before
272 the first rainfalls at the SOS. The onset of the rainy and dry season is estimated from crossing a defined
273 percentage threshold of the annual amplitude (AMP) value. Whereas the standard value of 20% has proven
274 to deliver robust results for the SOS (Horion et al., 2014), the EOS is influenced by several factors and needs
275 to be selected with caution. In addition to woody vegetation, the presence of crops can impact the early dry
276 season signal, since some crops (e.g. millet) remain greener 2-4 weeks longer than the annual grasses. To
277 better separate the core rainy season from influences, the threshold for the EOS was set to 80% of the
278 amplitude (Fig. 4). As we expect to capture the contribution of woody plants with the DSINT variable, an
279 integration period starting approximately mid-October is also preferable since some woody plant populations
280 are dominated by short deciduous species (e.g. *Acacia seyal*) shedding their leaves in the early dry season
281 (Fig. 3). To account for unreliable values extracted in areas of very low vegetation (as no distinct seasonal
282 curve is present for such areas), the woody cover of all pixels with a mean maximum annual FAPAR <0.05
283 and a stddev <0.02 was set to 0.5% (the total absence of shrubs is unlikely at 1 km scale). Wetlands and
284 irrigated areas were masked by excluding areas of high FAPAR values >0.2 between late November and
285 February, as only wetlands and irrigated croplands stay dark green during this time.

286

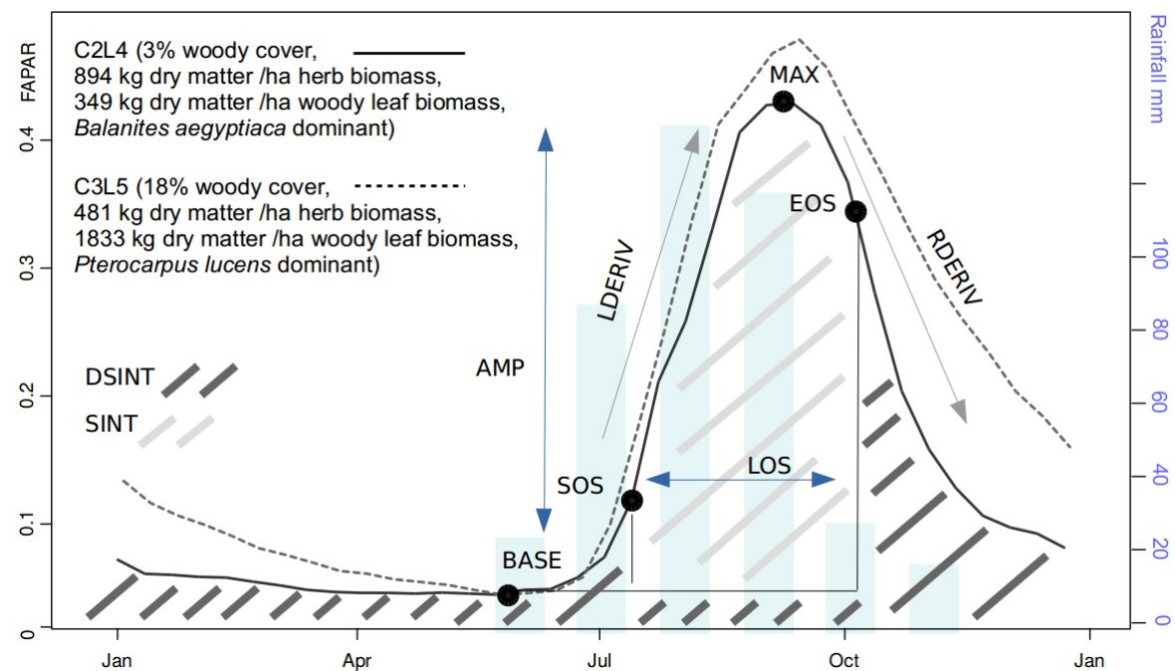
287

288 Table 1: Earth observation seasonal metrics used in this study (see Fig. 4 for illustrations).

Variable	Abbreviation	Definition
Base value	BASE	Minimum value over the season
Maximum value	MAX	Highest data value over the season
Amplitude	AMP	Difference between MAX and BASE
Small integral	SINT	Integral from SOS to EOS only values above BASE
Start of Season	SOS	Starting point of the growing season (20% of Amplitude)
End of Season	EOS	Ending point of the growing season (80% of Amplitude)
Length of Season	LOS	Time between SOS and EOS
Left derivative	LDERIV	Rate of increase before MAX
Right derivative	RDERIV	Rate of decrease after MAX
Dry season integral	DSINT	Annual integral – SINT

289

290



291

292 Figure 4: Annual VGT FAPAR cycle of pixels with sparse and moderately dense woody cover: The two ground sites
 293 (named C2L4 and C3L5) have contrasting values regarding woody cover, herb biomass and woody leaf biomass. All
 294 values are averaged over 1999-2013. Biomass data are taken from Brandt et al. (2015). For abbreviations, see Table 1.
 295 Whereas SINT represents the herbaceous layer, DSINT is proposed to reflect the woody layer.

296

297

298

299

300 ***Signature of woody cover in the seasonal FAPAR curve***

301 The variation over the year of FAPAR (mean 1999-2013) was compared for two sites of contrasting
302 herbaceous/woody vegetation dominance within the same rainfall regime in Senegal (Figure 4). The site
303 C2L4 has a high annual herbaceous biomass (~900 kg dry matter/ha) but low annual woody plant leaf
304 biomass production (~350 kg dry matter/ha) whereas site C3L5 is characterized by high annual woody plant
305 leaf biomass (~1850 kg dry matter/ha) and low annual herb biomass production (~500 kg dry matter/ha)
306 (Brandt et al., 2015). Seasonal dynamics of herbaceous vegetation are closely related to the pulse of rainfall,
307 and shortly after the herbaceous vegetation maximum (MAX) occurs, senescence starts (around late
308 September). Thus, after the FAPAR values drop following the MAX, woody plants determine the shape of
309 FAPAR curve until the following rainy season. This is illustrated by the high FAPAR values and slow
310 descending rate in the early dry season (October-December) in C3L5 (18% woody cover), as compared to
311 the rapidly decreasing FAPAR in C2L4 (3% woody cover) (Fig. 4). Moreover, despite a large difference in
312 total green mass during the wet season (1071 kg dry matter/ha difference), the maximum and amplitude of
313 FAPAR for the two sites are relatively similar. This shows that the woody plant foliage mass has a lower
314 impact on the annual FAPAR signature as compared to the herbaceous mass, and especially the rainy season
315 months are clearly dominated by the herbaceous cover (see supplementary material for all 43 ground sites).
316 The BASE level again is almost the same at both sites in spite the difference in woody cover, as the
317 deciduous woody plants at C3L5 shed their leaves in the dry season, whereas the evergreen woody
318 vegetation at C2L4 keeps the green leaves throughout the year leading to a stable BASE level. The different
319 phenological behaviors shown in Fig. 3 are reflected in the FAPAR curves of Fig. 4.

320

321 ***Variables selection for woody cover modeling***

322 A multiple linear regression model was established between *in situ* measured observations (*cWC*) from
323 Senegal and Mali, and seasonal metrics derived from VGT and MODIS FAPAR satellite data. To avoid

324 overfitting and find the minimal adequate model, the number of variables shown in Table 1 was reduced.
325 Multicollinearity is known to bias parameters of variable selection and is commonly found for variables
326 influenced by seasonality. The Variable Inflation Factor (VIF) was calculated and used to test all metrics
327 included in the model for multicollinearity and for removal of highly correlated predictors. The remaining
328 metrics were used in a stepwise regression run in a backward direction, a technique which reduces the
329 number of variables in each step (Chambers and Hastie, 1991). Here, the AIC (Akaike Information Criterion)
330 was used to identify and remove metrics that decreased the overall model quality. The relative contributions
331 of the predictors to the model's total explanatory power were estimated by the LMG (Lindeman, Merenda
332 and Gold) method (a bootstrap measure based on 100 samples) as described in Grömping (2007). This
333 method provides the explaining power of each metric in the model as a share of 100%.

334

335 ***Woody cover model validation and evaluation***

336 Models with a limited number of observations and a high number of predictors are sensitive to unreliable
337 statistical parameter retrieval (Zandler et al., 2014) and therefore 3 parameters were applied for model
338 validation:

339

- 340 1. *Adjusted r^2* , which is raw r^2 adjusted to the number of explaining variables in a multiple regression.
341 The adjusted r^2 is susceptible to overfitting but widely used as a common and comparable variable
342 for model validation.
- 343 2. A *predictive r^2* is applied to assess the shrinkage of raw r^2 and the predicting ability of the model,
344 dealing with the overfitting problem (Allen, 1974). The predictive r^2 is based on a cross validation
345 called PRESS (predicted residual sum of squares). Unlike the often used bootstrapping technique
346 providing a measure of a model's uncertainty, PRESS provides a measure of the model's prediction
347 ability by predicting a number of observations that were not used to establish the model.
- 348 3. A *cross validation* is applied to assess a model's predictive error rate and the cross validated Root
349 Mean Square Error (cvRMSE) in % woody cover. The data are randomly assigned to four equally
350 sized subsamples (called folds), each using k random ground monitoring sites. Each fold is removed,
351 while the remaining data is used to re-fit the regression model and to predict the deleted

352 observations. The root of the mean squares of all folds gives the cvRMSE.

353

354 ***Extrapolation of woody cover to Sahel scale***

355 Since the model was established with corrected woody cover (cWC) representing the dry season green mass
356 adjusted to foliage phenology, the retrieval of the total woody cover at Sahel scale required the adjustment of
357 the canopy cover derived from phenological metrics by the estimated mean foliage density of woody
358 canopies during dry season across the whole Sahel. This mean foliage density was assessed by estimating the
359 relative contribution of the six woody plant foliage phenotypes within each of the three bioclimatic zones
360 and then weighted them by mean canopy cover within each zones (Fig. 6). It resulted of a mean foliage
361 density value of 0.63. For extrapolation to Sahel scale, the predicted values were thus divided by 0.63 to
362 inverse the correction and retrieve the total woody cover. Negative predictions were set to zero.

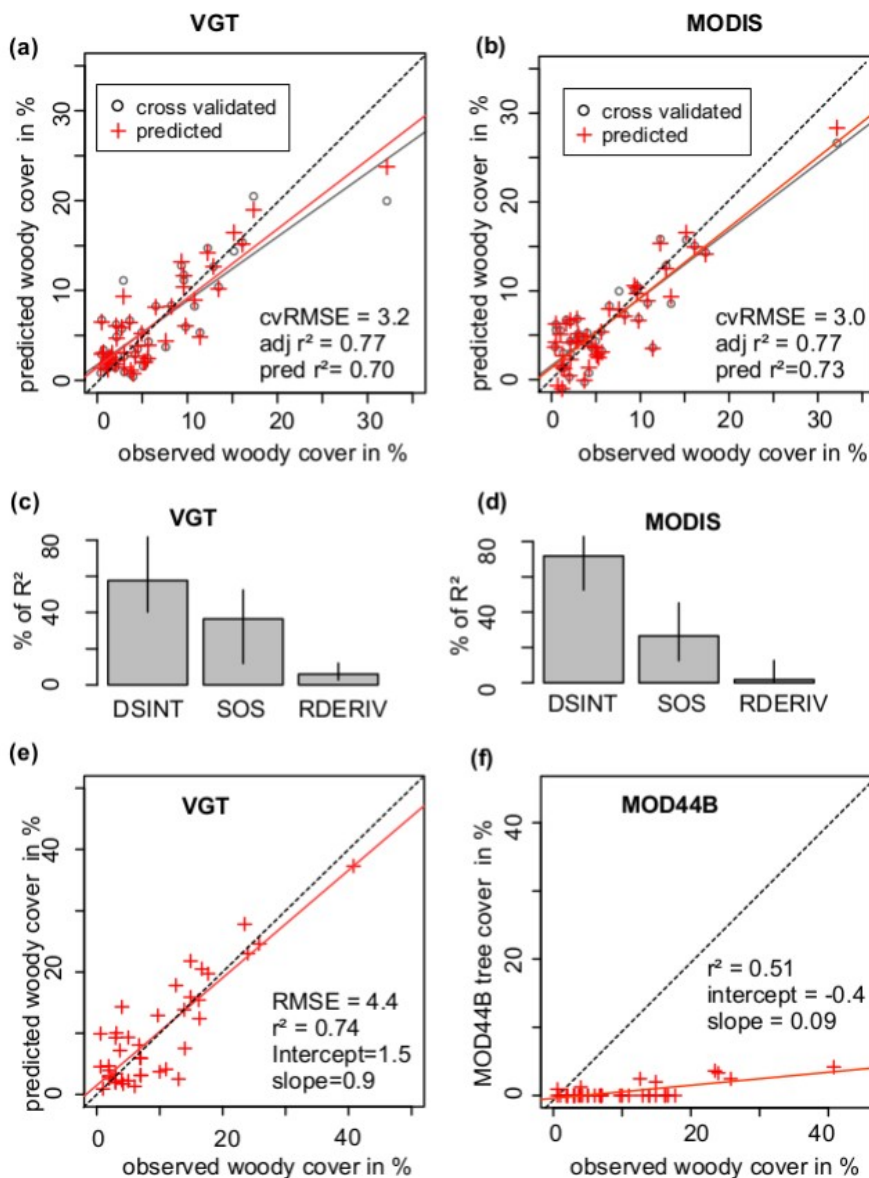
363

364 **Results**

365 ***Selecting satellite metrics related to woody cover***

366 In spite of the differences in the original FAPAR datasets, the variables with the highest predictive capacity
367 being selected in the multilinear models were the same from both VGT and MODIS phenological metrics. In
368 a first step, metrics causing a high VIF in both VGT and MODIS models were removed (length of the season
369 LOS and SINT, see correlation matrix in supplementary material for details on interrelationships). The
370 subsequent stepwise regression removed first the AMP and MAX metrics which are both primarily
371 controlled by the herbaceous growth. In the final round, the BASE, the increasing rate (LDERIV) and the
372 EOS were removed. Although a relation to corrected woody cover exists for these metrics, other metrics
373 show a higher importance for the overall prediction accuracy of the model and the remaining metrics in the
374 final models were DSINT, SOS, and RDERIV with a VIF <2 and significance <0.01 for both VGT and
375 MODIS FAPAR (Fig. 5). While RDERIV provides information on the period of decreasing influence of
376 green herbaceous vegetation on the FAPAR curve, the SOS is as well related to the leafing of trees, as many
377 woody species start their leafing before the onset of the rainy season (Fig. 3), triggered by air temperature
378 and relative humidity. This is especially the case in the southern Sahel, where woody plants develop leaves
379 markedly ahead of the first rainfall events (in contrast to herbaceous vegetation dependent on an increase in

380 soil moisture for massive germination) (Devineau, 1999), attributing the first increasing FAPAR signal after
 381 the dry season to woody plants. As only woody species remain green over parts of the dry season, the BASE
 382 could be considered as another important predictor (Horion *et al.*, 2014), however, this variable did not
 383 improve the predictions of the models. DSINT represents the FAPAR integral from the onset of the dry
 384 season to the onset of the following rainy season, which is a distinctive period for woody leafing and thus
 385 our most important and robust variable. DSINT is found to explain around 60% and 80% of the r^2 in the
 386 VGT and MODIS models respectively (Fig. 5c,d) (metrics are normalized to sum 100%).



387 *Figure 5: Accuracy assessment, prediction and metric importance (a) for SPOT VGT and (b) for MODIS. The predicted*
 388 *(multiple regression model) and cross-validation predicted values (using 4 subsamples to predict points not used to*
 389 *establish the model) are plotted against corrected in situ data. CvRMSE is given in % woody cover. (c) Relative*

390 importance of the variables used to predict corrected woody cover with 95% bootstrap confidence intervals for SPOT
391 VGT and (d) for MODIS. LMG method is used (Grömping, 2007) and metrics are normalized to sum 100%. For
392 abbreviations, see Table 1. (e) Uncorrected in situ data is plotted against predicted data after multiplication with the
393 coefficient (only VGT is shown). (f) Compares in situ data woody cover with MOD44B tree cover.

394

395

396 ***Validation of the woody cover models and comparison with MOD44B tree cover***

397 The error rates for both the VGT and MODIS models are very low ($cvRMSE = 3.2$ and 3.0% woody cover
398 respectively) and the prediction ability of the models high (Fig. 5a,b) with a predictive r^2 of 0.73 (MODIS)
399 and 0.70 (VGT). Only one field site of continuous measurements exists in the densely vegetated southern
400 parts (woody cover of approximately 40%). As such this point stands out in the scatterplots (Fig. 5) and
401 ideally should be complemented with additional measurements of dense woody cover for improved model
402 confidence in areas of 30-40% woody cover. The MOD44B global tree cover product (not considering
403 shrubs) shows a low agreement with the predicted and measured woody cover (Fig. 5f and Table 2). Even
404 though a significant linear relationship between ground observations and MOD44B is present ($r^2=0.51$,
405 $p<0.01$), the percentage tree cover estimate by MOD44B is generally much lower than the woody cover *in*
406 *situ* data from Senegal and Mali with an underestimation of a factor of 8.8 (slope=0.09, intercept=-0.4). This
407 supports that the MOD44B tree canopy cover product delivers only partial information on the total woody
408 canopy cover.

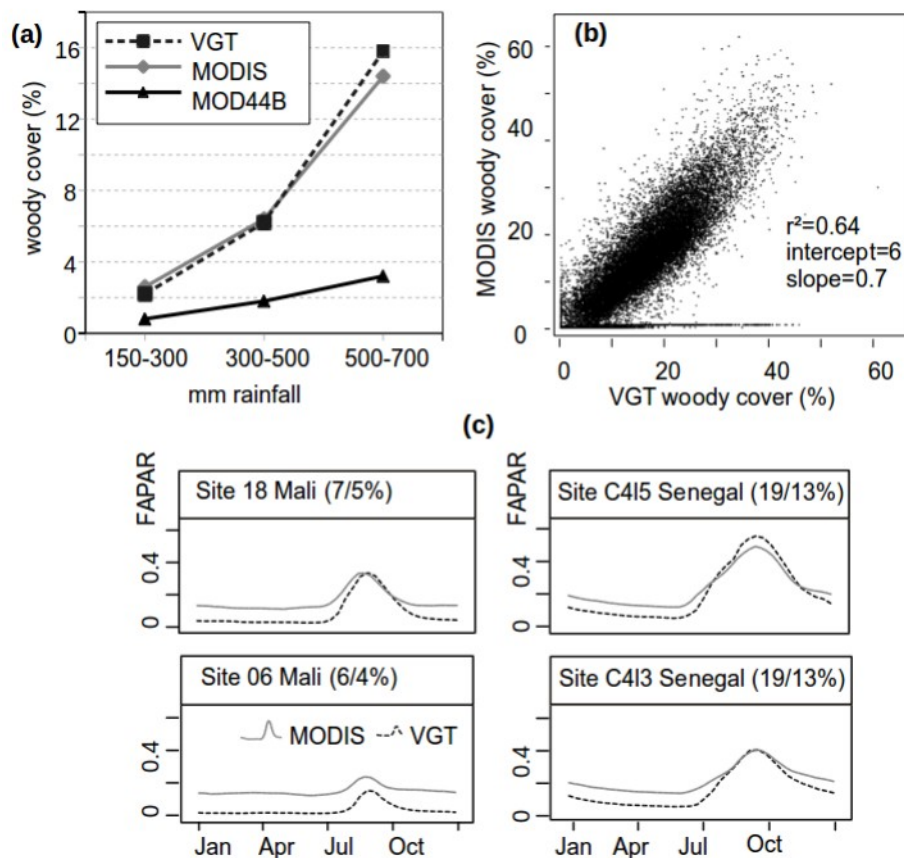
409

410

411 ***Extrapolation and comparison between SPOT VGT and MODIS FAPAR***

412 The uncertainty of the estimated woody cover increases after extrapolation division by the mean foliage
413 density of the canopy cover during the dry season, however, at the same time, the slope increases (Fig. 5e).
414 The extrapolated canopy cover of woody plants averages $7.3 \pm 7.8\%$ (VGT), $7.0 \pm 8.3\%$ (MODIS) over the
415 whole Sahel belt. At the regional scale, the canopy cover decreases with mean annual rainfall (Table 2, Fig
416 6a) as expected from threshold relationship established globally (Sankaran et al., 2005). Mean woody cover
417 in the three bioclimate sub-zones delineated by the isohyets 300 and 500 mm (Fig. 2) are clearly related to

418 rainfall (Fig. 6a). Generally, both VGT and MODIS based FAPAR satellite datasets are able to predict the
 419 ground observations fairly accurate using the same set of metrics. MODIS FAPAR derived model has
 420 slightly better values (Fig. 5), but the FAPAR product includes several no-data pixels pre-classified as
 421 “barren land” over the entire time period. These are excluded when calculating the mean FAPAR in the
 422 polygons of the ground site areas, but set to 0.5% woody cover in the final extrapolated map. These barren
 423 land pixels not only appear in the northern Sahel masking desert areas, but also 4.1% of the southern parts
 424 (500-700 mm rainfall) with dense woody cover are erroneously pre-classified as barren land in the
 425 MOD15A2 dataset. These pixels have woody cover up to 40% in the VGT map and prevent a higher
 426 correlation between VGT and MODIS woody cover ($r^2=0.64$) (Fig. 6b). Moreover, Fig. 6c shows a
 427 systematic gap between dry season VGT and MODIS values, especially in sparsely vegetated areas.



428
 429 *Figure 6: (a) Means of pixel values for woody cover by mean rainfall zones (Fig. 2) as derived from VGT, MODIS*
 430 *FAPAR, or from the MOD44B product. (b) VGT and MODIS woody cover over the Sahel (plot uses a sample of 3% of*
 431 *the cells) showing that pre-classified barren land in MODIS has woody cover up to 40% in VGT, preventing a higher*
 432 *correlation. (c) Temporal FAPAR profiles of 4 ground sites showing (1) that the impact of uncorrected woody*

433 cover/corrected woody cover (%) on the rainy season metrics is of minor importance and (2) the systematic gap
434 between MODIS and VGT, with MODIS overestimating the dry season FAPAR especially in sparsely vegetated areas.

435

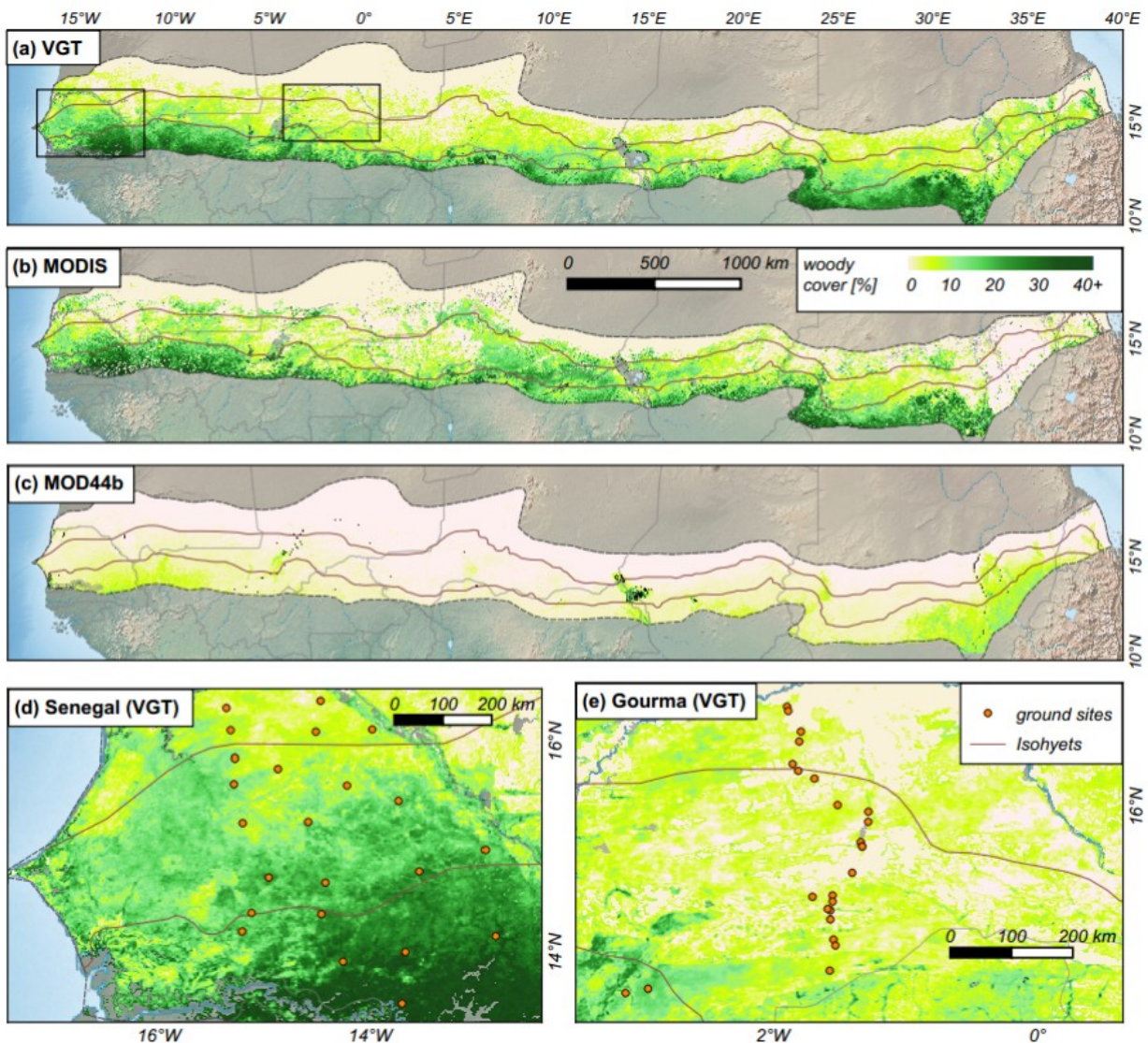
436 Table 2: Pixel statistics at Sahel scale for the woody cover maps derived from VGT, MODIS FAPAR and MOD44B (as
437 seen in Fig. 7a-c) for three different rainfall zones shown in Figure 2. Mean and SD are given in woody cover %. Values
438 refer to all pixels available for the three compared products.

439

440

Rainfall	VGT		MODIS		MOD44B	
	mean	SD	mean	SD	mean	SD
150-300 mm	2.2	2.9	2.6	4.5	0.8	11
300-500 mm	6.0	4.9	6.2	5.9	1.8	13
500-700 mm	15.4	7.9	13.8	9.7	3.2	11.7

441



442 Figure 7: Extrapolated woody cover maps derived from VGT (a) and MODIS (b) FAPAR as well as the global tree cover
 443 product MOD44B (c). (d+e) show zooms to Senegal and Gourma (Mali) using VGT map (the squares in (a)). Masked
 444 wetlands are displayed gray.

445

446

447 **Discussion**

448 ***Differences between woody/tree cover maps***

449 A method based on seasonal metrics is able to estimate woody cover within 1 km pixels, relating the
 450 specific intra-annual shape of the FAPAR curve with ground measured canopy cover and phenological
 451 behavior. The FAPAR derived maps differ slightly between VGT and MODIS. The land cover dependent
 452 inversion in MODIS approach may introduce some bias in MODIS estimates which overestimate low

453 FAPAR values over sparsely vegetated areas (McCallum et al., 2010; Fensholt et al., 2004; Martinez et al.,
454 2013). This overestimation leads to a higher woody cover in parts of the northern fringe of the study area in
455 comparison to VGT with values between 10 and 20% (Fig. 7b), which is unlikely in the 150-300 mm rainfall
456 zone.

457 Our results significantly differ from the global tree cover product MOD44B, with an almost nine times
458 higher canopy cover in our maps and ground observations. The same is true for the Landsat based map
459 developed by Sexton et al. (2013) (not shown for brevity). This supports existing studies (Herrmann et al.,
460 2013; Gessner et al., 2013) which detect a generally very low tree cover in global products over the Sahel. It
461 further demonstrates that, although the spatial pattern in the MOD44B product is similar and the relation
462 linear to ground data, MOD44B delivers only partial information on the total woody cover in semi-arid
463 drylands, omitting small trees, shrubs and bushes. Our plant phenology and FAPAR metrics based approach
464 constitutes an improvement by capturing all woody plants isolated or in thickets.

465

466 *Characteristics of the FAPAR based Sahel maps*

467 The regional distribution of the woody cover is explained by the rainfall gradient. More locally, soil type
468 and the pattern of rain water redistribution by run-off interfere with land-use to explain for contrasted woody
469 cover. Compared to the dominant permeable sandy soils, upland rocky areas, iron pan outcrops and shallow
470 soils are either bare (below the FAPAR threshold) or else tend to have higher woody cover than surrounding
471 lands. Such bare rocky areas occur in the Tagant and the Dhar Nema in Mauritania, the erosion surfaces of
472 the Gourma region ('assalwa', Ag Mahmoud 1992), over the Oulliminden plateau in Niger, while rocky hills
473 such as the Affolé in Mauritania, the Mandingo, Bandiagara and Gandamia plateaus in Mali, Ader Douchi in
474 Niger and Mount Guedi in Chad have higher woody cover than surrounding plains. Perhaps steep slopes and
475 shadows contribute to this local overestimation.

476 The web of valleys is almost systematically underlined by higher woody cover than surroundings. It is
477 particularly obvious for the Baoulé and Bakoye rivers in Mali, the Goulbin and Komadougou in Niger and
478 northern Nigeria, but also the Batha in Chad, and wadies from the Darfur in Sudan. In a few cases however,
479 valleys duly appear with lower canopy cover: the Snake river in Mali, Bahr El Ghazal in Chad. Land use also
480 explains for local patterns e.g. higher woody density in forest reserves having sharp boundaries with

481 surrounding cropland as in Mbégué in Senegal, Tangaza in northern Nigeria, Baban Rafi in Niger. In spite of
482 the tall trees of the agrarian parkland, woody cover is generally less at the vicinity of the villages than further
483 away with larger extends of bushy fallows. This pattern centered on villages clearly applies to Baol in
484 Senegal, Séno Gondo in Mali, Gobir and Mandaram in Niger and northern Kordofan in Sudan. Towns are
485 often mapped as bare land, however, especially down town areas in bigger cities have enough tree along
486 streets or in gardens to be classified with low woody cover.

487

488 *Uncertainties, sources of error and proposed improvements*

489 Our extrapolated woody cover map is not claimed to be without errors and several points have to be
490 considered: (1) Despite masking the Sudanian area in the south, vegetation in the semi-arid southern parts of
491 the Sahel behaves differently as compared to the vegetation in the dry northern parts. Although annuals are
492 still dominating at the 700 mm rainfall border, perennials can be present and do normally not wilt before
493 October-November. Moreover, the dry season phenology is defined from October to June, which is an
494 approximation for the overall research area. The method is however robust, which can be explained by the
495 start and end of season dissymmetry with limited spread of the date of end of the rainy season along the
496 gradient (late September to mid-October) and wider spread of the onset of the wet season (May to July), a
497 period of the year with low density of leaves. (2) No ground data exists from cropping areas, which limits the
498 accuracy of the model developed in these areas. Cropping areas have a slow FAPAR onset at the start of the
499 rainy season and a delayed growth that may also overlap in October-November. (3) Most wetlands have been
500 masked (e.g. the Niger delta, Senegal river, lake Chad), but smaller areas remain and woody cover
501 estimations in flooded wetlands are biased by herbaceous species staying green after the rainy season and
502 regrow soon after. (4) Fire is a common ecosystem feature in the Sahel and especially southern areas are
503 regularly burned. Fires usually occur during the dry season and re-sprouting of perennials in southern areas
504 can impact the FAPAR baseline long after the last rainfall event. (5) The characteristics of the ground sites in
505 Senegal and Mali used for the calibration of the models and the mean foliage density used for the
506 extrapolation may not be representative of all the local characteristics and diversity of woody population
507 landscapes in the Sahel. This can be seen in the increased uncertainty after adding the coefficient after
508 extrapolation. The application of one mean foliage density value (0.63) for all types of phenology adds a

509 degree of uncertainty. For example, an evergreen (e.g. *C. glutinosum*, *B. aegyptiaca*) dominated stand would
510 have a foliage density of 0.78, whereas semi-deciduous sites (*G. senegalensis*) have 0.71, and medium
511 deciduous 0.28 (*P. lucens*). Completely short deciduous stands (*A. seyal*) would even have a foliage density
512 of 0.08, however, at a 1 km scale this rarely occurs in the Sahel and most pixels have a mixed woody
513 population.

514

515 Ground and satellite data are biased by sampling errors and processing uncertainties, respectively and the
516 ground measurements are not continuous and free of gaps in the temporal domain, excluding an exact
517 adaptation to the satellite data period. Thus, a temporal average over a longer period was chosen here to
518 guarantee an unbiased relationship between *in-situ* and EO data. By setting a fixed woody cover value of
519 0.5% in areas with a very low maximum and stdev of FAPAR, unrealistic vegetation metric outputs were
520 mostly excluded. This is a precaution measure since the methodology presented is not able to produce
521 reliable results in these areas due to curve-fitting limitations and intrinsic limitations to the use of EO data
522 for vegetation monitoring in areas of very sparse vegetation cover. For a better prediction and to reduce
523 mentioned issues, multiple metrics should be selected for different plant functional types. Further
524 improvements can be made by including vegetation and land cover maps to derive different types of models
525 and inversion coefficients using different metrics and calibrations, depending on the dominating woody
526 species and soil (Diouf et al., 2015). Moreover, land use maps could adjust the model to differences in plant
527 phenology between cropland, rangeland and forest areas. “Finally, to produce annual maps of woody cover
528 changes over time, the method has to be robust against inter-annual fluctuations of satellite derived metrics
529 (Broich et al., 2015) caused by rainfall dynamics, human disturbances (cutting, clearing), fires and especially
530 dynamics of leaf density hiding the real trend in woody population changes.”

531

532

533 **Conclusion**

534

535 An Earth Observation based model of woody cover in the Sahelian drylands was developed from seasonal
536 vegetation metrics and 20 years of *in situ* measured woody cover at 43 sites. The concept of the model was

537 developed from *a priori* knowledge of the significantly different phenophases of the persistent (woody
538 cover) and recurrent (herbaceous) vegetation, with annual herbaceous vegetation being photosynthetically
539 active only during the rainy season whereas most trees and shrubs remain active over large parts of the year.
540 Our estimation of the total canopy cover of all woody phanerophytes shows an almost nine times higher
541 cover than an existing global tree cover product. This suggests that in a semi-arid dryland dominated by
542 shrubs and small trees, a phenology based approach is a significant improvement and an important
543 contribution for future studies quantifying carbon stocks, climate change assessment as well as
544 parametrization of vegetation dynamic models. Although temporal changes and dynamics were not
545 addressed within this study (in the interest of developing a robust and stable relationship between ground
546 observations and satellite data), the knowledge on the established relationships is applied in an ongoing
547 study monitoring woody dynamics in the Sahel area. The woody cover dataset is made publicly available
548 (following the example of Broich et al., 2015) for download (information on the data access can be found in
549 the supplementary material).

550

551 **Acknowledgements**

552

553 The authors thank everyone involved in collecting the ground data in Senegal and Mali, especially the Centre
554 de Suivi Ecologique (CSE), Dakar. The project (BICSA) leading to this application has received funding
555 from the European Union's Horizon 2020 research and innovation programme under the Marie Skłodowska-
556 Curie grant agreement No [656564]. The study was further supported by the Danish Council for Independent
557 Research (DFF) Sapere Aude programme, and the European Earth observation programme Copernicus
558 Global land and GIOBIO (32-566) project. Alexandre Verger is the recipient of a *Juan de la Cierva*
559 postdoctoral fellowship from the Spanish Ministry of Science and Innovation. A.A. Diouf is supported by the
560 AGRICAB project (Contract No. 282621), funded by the European Union under the seventh Framework
561 Programme (FP7). Finally we thank Laurent Kergoat and the two anonymous reviewers for useful comments
562 on the manuscript.

563

564

565 **References**

566

567 Ag Mahmoud, M., 1992. Le haut Gourma Central, 2nd edn., edited by: Le Floc'h, R., CEFE/CNRS,
568 Montpellier, 133 pp.

569

570 Allen, D.M., 1974. The Relationship between Variable Selection and Data Augmentation and a Method for
571 Prediction. *Technometrics* 16, 125–127. doi:10.2307/1267500

572

573 Barbé, L.L., Lebel, T., 1997. Rainfall climatology of the HAPEX-Sahel region during the years 1950–1990.
574 *Journal of Hydrology, HAPEX-Sahel* 188–189, 43–73. doi:10.1016/S0022-1694(96)03154-X

575

576 Baret, F., Hagolle, O., Geiger, B., Bicheron, P., Miras, B., Huc, M., Berthelot, B., Weiss, M., Samain, O.,
577 Roujean, J.L., & Leroy, M. (2007). LAI, fAPAR and fCover CYCLOPES global products derived from
578 VEGETATION. Part 1: Principles of the algorithm. *Remote Sensing of Environment*, 110, 275-286

579

580 Baret, F., Weiss, M., Lacaze, R., Camacho, F., Makhmara, H., Pacholczyk, P., Smets, B., 2013. GEOV1: LAI
581 and FAPAR essential climate variables and FCOVER global time series capitalizing over existing products.

582 Part1: Principles of development and production. *Remote Sensing of Environment* 137, 299–309.

583 doi:10.1016/j.rse.2012.12.027

584

585 Brandt, M., Mbow, C., Diouf, A.A., Verger, A., Samimi, C., Fensholt, R., 2015. Ground- and satellite-based
586 evidence of the biophysical mechanisms behind the greening Sahel. *Glob Change Biol* 21, 1610–1620.

587 doi:10.1111/gcb.12807

588

589 Broich, M., Huete, A., Tulbure, M.G., Ma, X., Xin, Q., Paget, M., Restrepo-Coupe, N., Davies, K., Devadas,
590 R., Held, A., 2014. Land surface phenological response to decadal climate variability across Australia using

591 satellite remote sensing. *Biogeosciences* 11, 5181–5198. doi:10.5194/bg-11-5181-2014

592

593 Broich, M., Huete, A., Paget, M., Ma, X., Tulbure, M., Restrepo-Coupe, N., Evans, B., Beringer, J.,
594 Devadas, R., Davies, K., others, 2015. A spatially explicit land surface phenology data product for science,
595 monitoring and natural resources management applications. *Environmental Modeling and Software*.
596

597 Chambers, J.M., Hastie, T.J. (Eds.), 1991. *Statistical Models in S*. Chapman and Hall/CRC, Boca Raton, Fla.
598

599 Dardel, C., Kergoat, L., Hiernaux, P., Mougin, E., Grippa, M., Tucker, C.J., 2014. Re-greening Sahel:
600 30 years of remote sensing data and field observations (Mali, Niger). *Remote Sensing of Environment* 140,
601 350–364. doi:10.1016/j.rse.2013.09.011
602

603 De Bie, S., Ketner, P., Paasse, M., Geerling, C., 1998. Woody plant phenology in the West Africa savanna.
604 *Journal of Biogeography* 25, 883–900. doi:10.1046/j.1365-2699.1998.00229.x
605

606 Defries, R.S., Hansen, M.C., Townshend, J.R.G., Janetos, A.C., Loveland, T.R., 2000. A new global 1-km
607 dataset of percentage tree cover derived from remote sensing. *Global Change Biology* 6, 247–254.
608 doi:10.1046/j.1365-2486.2000.00296.x
609

610 Devineau, J.-L., 1999. Seasonal Rhythms and Phenological Plasticity of Savanna Woody Species in a Fallow
611 Farming System (South-West Burkina Faso). *Journal of Tropical Ecology* 15, 497–513.
612

613 Diouf, A.A., Brandt, M., Verger, A., Jarroudi, M.E., Djaby, B., Fensholt, R., Ndione, J.A., Tychon, B., 2015.
614 Fodder Biomass Monitoring in Sahelian Rangelands Using Phenological Metrics from FAPAR Time Series.
615 *Remote Sensing* 7, 9122–9148. doi:10.3390/rs70709122
616

617 Fensholt, R., Rasmussen, K., Kaspersen, P., Huber, S., Horion, S., Swinnen, E., 2013. Assessing Land
618 Degradation/Recovery in the African Sahel from Long-Term Earth Observation Based Primary Productivity
619 and Precipitation Relationships. *Remote Sensing* 5, 664–686. doi:10.3390/rs5020664
620

621 Fensholt, R., Sandholt, I., Rasmussen, M.S., 2004. Evaluation of MODIS LAI, fAPAR and the relation
622 between fAPAR and NDVI in a semi-arid environment using in situ measurements. *Remote Sensing of*
623 *Environment* 91, 490–507. doi:16/j.rse.2004.04.009

624

625 Gessner, U., Machwitz, M., Conrad, C., Dech, S., 2013. Estimating the fractional cover of growth forms and
626 bare surface in savannas. A multi-resolution approach based on regression tree ensembles. *Remote Sensing*
627 *of Environment* 129, 90–102. doi:10.1016/j.rse.2012.10.026

628

629 Grömping, U., 2007. Estimators of Relative Importance in Linear Regression Based on Variance
630 Decomposition. *The American Statistician* 61, 139–147. doi:10.1198/000313007X188252

631

632 Hansen, M.C., DeFries, R.S., Townshend, J.R.G., Carroll, M., Dimiceli, C., Sohlberg, R.A., 2003. Global
633 Percent Tree Cover at a Spatial Resolution of 500 Meters: First Results of the MODIS Vegetation
634 Continuous Fields Algorithm. *Earth Interact.* 7, 1–15. doi:10.1175/1087-
635 3562(2003)007<0001:GPTCAA>2.0.CO;2

636

637 Hansen, M.C., DeFries, R.S., Townshend, J.R.G., Marufu, L., Sohlberg, R., 2002. Development of a MODIS
638 tree cover validation data set for Western Province, Zambia. *Remote Sensing of Environment* 83, 320–335.

639

640 Hansen, M.C., Townshend, J.R.G., DeFries, R.S., Carroll, M., 2005. Estimation of tree cover using MODIS
641 data at global, continental and regional/local scales. *International Journal of Remote Sensing* 26, 4359–4380.
642 doi:10.1080/01431160500113435

643

644 Herrmann, S., Wickhorst, A., Marsh, S., 2013. Estimation of Tree Cover in an Agricultural Parkland of
645 Senegal Using Rule-Based Regression Tree Modeling. *Remote Sensing* 5, 4900–4918.
646 doi:10.3390/rs5104900

647

648 Hiernaux P., Cissé, M. I., Diarra, L., de Leeuw P. N., 1994. Fluctuations saisonnières de la feuillaison des

649 arbres et buissons sahéliens. Conséquences pour la quantification des ressources fourragères. Revue
650 d'Élevage et de Médecine Vétérinaire des Pays Tropicaux 47, 117-125.

651 Hiernaux, P., Diarra, L., Trichon, V., Mougin, E., Soumaguel, N., Baup, F., 2009. Woody plant population
652 dynamics in response to climate changes from 1984 to 2006 in Sahel (Gourma, Mali). Journal of Hydrology
653 375, 103–113. doi:16/j.jhydrol.2009.01.043

654

655 Hiernaux, P., Le Houérou, H.N., 2006. Les parcours du Sahel. Sécheresse, 17(1-2): 51-71

656

657 Horion, S., Fensholt, R., Tagesson, T., Ehammer, A., 2014. Using earth observation-based dry season NDVI
658 trends for assessment of changes in tree cover in the Sahel. International Journal of Remote Sensing 35,
659 2493–2515. doi:10.1080/01431161.2014.883104

660

661 Jobard, I., Chopin, F., Berges, J.C., Roca, R., 2011. An intercomparison of 10-day satellite precipitation
662 products during West African monsoon. International Journal of Remote Sensing 32, 2353–2376.
663 doi:10.1080/01431161003698286

664

665 Jönsson P, Eklundh L (2004) TIMESAT - a program for analyzing time-series of satellite sensor data.
666 *Computers & Geosciences*, **30**, 833-845.

667

668 Karlson, M., Reese, H., Ostwald, M., 2014. Tree Crown Mapping in Managed Woodlands (Parklands) of
669 Semi-Arid West Africa Using WorldView-2 Imagery and Geographic Object Based Image Analysis. Sensors
670 14, 22643–22669. doi:10.3390/s141222643

671

672 Le Houérou HN. (1980). The Rangelands of the Sahel. *J Range Manage*, 33, 41-6.

673

674 Martínez, B., Camacho, F., Verger, A., García-Haro, F.J., Gilabert, M.A., 2013. Intercomparison and quality
675 assessment of MERIS, MODIS and SEVIRI FAPAR products over the Iberian Peninsula. International

676 Journal of Applied Earth Observation and Geoinformation 21, 463–476. doi:10.1016/j.jag.2012.06.010

677

678 Mbow, C., Chhin, S., Sambou, B., Skole, D., 2013. Potential of dendrochronology to assess annual rates of
679 biomass productivity in savanna trees of West Africa. *Dendrochronologia* 31, 41–51.

680 doi:10.1016/j.dendro.2012.06.001

681

682 McCallum, I., Wagner, W., Schmullius, C., Shvidenko, A., Obersteiner, M., Fritz, S., Nilsson, S., 2010.

683 Comparison of four global FAPAR datasets over Northern Eurasia for the year 2000. *Remote Sensing of*

684 *Environment* 114, 941–949. doi:10.1016/j.rse.2009.12.009

685

686 Mougin, E., Demarez, V., Diawara, M., Hiernaux, P., Soumaguel, N., Berg, A., 2014. Estimation of LAI,

687 fAPAR and fCover of Sahel rangelands (Gourma, Mali). *Agricultural and Forest Meteorology* 198–199,

688 155–167. doi:10.1016/j.agrformet.2014.08.006

689

690 Mougin, E., Hiernaux, P., Kergoat, L., Grippa, M., de Rosnay, P., Timouk, F., Le Dantec, V., Demarez, V.,

691 Lavenu, F., Arjounin, M., Lebel, T., Soumaguel, N., Ceschia, E., Mougnot, B., Baup, F., Frappart, F.,

692 Frison, P.L., Gardelle, J., Gruhier, C., Jarlan, L., Mangiarotti, S., Sanou, B., Tracol, Y., Guichard, F., Trichon,

693 V., Diarra, L., Soumaré, A., Koité, M., Dembélé, F., Lloyd, C., Hanan, N.P., Damesin, C., Delon, C., Serça,

694 D., Galy-Lacaux, C., Seghieri, J., Becerra, S., Dia, H., Gangneron, F., Mazzega, P., 2009. The AMMA-

695 CATCH Gourma observatory site in Mali: Relating climatic variations to changes in vegetation, surface

696 hydrology, fluxes and natural resources. *Journal of Hydrology* 375, 14–33. doi:10.1016/j.jhydrol.2009.06.045

697

698 Mougin, E., Lo Seen, D., Rambal, S., Gaston, A., Hiernaux, P., 1995. A regional Sahelian grassland model to

699 be coupled with multispectral satellite data. I: Model description and validation. *Remote Sensing of*

700 *Environment* 52, 181–193. doi:10.1016/0034-4257(94)00126-8

701

702 Myneni, R.B., Hoffman, S., Knyazikhin, Y., Privette, J.L., Glassy, J., Tian, Y., Wang, Y., Song, X., Zhang, Y.,

703 Smith, G.R., Lotsch, A., Friedl, M., Morisette, J.T., Votava, P., Nemani, R.R., & Running, S.W. (2002).

704 Global products of vegetation leaf area and absorbed PAR from year one of MODIS data. *Remote Sensing of*
705 *Environment*, 83, 214-231

706

707 Myneni, R.B., Williams, D.L., 1994. On the relationship between FAPAR and NDVI. *Remote Sensing of*
708 *Environment* 49, 200–211. doi:10.1016/0034-4257(94)90016-7

709

710 Rasmussen, K., Fog, B., Madsen, J.E., 2001. Desertification in reverse? Observations from northern Burkina
711 Faso. *Global Environmental Change* 11, 271–282. doi:16/S0959-3780(01)00005-X

712

713 Rasmussen, M.O., Göttsche, F.-M., Diop, D., Mbow, C., Olesen, F.-S., Fensholt, R., Sandholt, I., 2011. Tree
714 survey and allometric models for tiger bush in northern Senegal and comparison with tree parameters
715 derived from high resolution satellite data. *International Journal of Applied Earth Observation and*
716 *Geoinformation* 13, 517–527. doi:16/j.jag.2011.01.007

717

718 Rasmussen, K., Nielsen, T.T., Mbow, C., Wardell, A., 2006. Land degradation in the Sahel: An apparent
719 scientific contradiction, in: Møllegaard, M. (Ed.), *Natural Resource Management in Sahel – Lessons Learnt*,
720 *Occasional Paper : SEREIN, Sahel-Sudan Environmental Research Initiative. SEREIN, Sahel-Sudan*
721 *Environmental Research Initiative*, pp. 37–43.

722

723 Roujean, J.L., Leroy, M., & Deschamps, P.Y. (1992). A bidirectional reflectance model of the Earth's surface
724 for the correction of remote sensing data. *Journal of Geophysical Research*, 97, 20455-20468

725

726 San Emeterio, J.L., Mering, C., 2012. Climatic and human impacts on the ligneous cover in the Sahel from
727 analysis of aerial photographs before and after the drought periods of the 70's and 80's, in: *EGU General*
728 *Assembly Conference Abstracts. Presented at the EGU General Assembly Conference Abstracts*, p. 3052.

729

730 Sankaran, M., Hanan, N.P., Scholes, R.J., Ratnam, J., Augustine, D.J., Cade, B.S., Gignoux, J., Higgins, S.I.,

731 Le Roux, X., Ludwig, F., Ardo, J., Banyikwa, F., Bronn, A., Bucini, G., Caylor, K.K., Coughenour, M.B.,
732 Diouf, A., Ekaya, W., Feral, C.J., February, E.C., Frost, P.G.H., Hiernaux, P., Hrabar, H., Metzger, K.L.,
733 Prins, H.H.T., Ringrose, S., Sea, W., Tews, J., Worden, J., Zambatis, N., 2005. Determinants of woody cover
734 in African savannas. *Nature* 438, 846–849. doi:10.1038/nature04070
735
736 Sayre, R., Comer, P., Hak, J., Josse, C., Bow, J., Warner, H., Larwanou, M., Kelbessa, E., Bekele, T., Kahl,
737 H., Amena, R., Andriamasimanana, R., Ba, T., Benson, L., Boucher, T., Brown, M., Cress, J., Dassering, O.,
738 Friesen, B., Gachathi, F., Houcine, S., Keita, M., Khamala, E., Marangu, D., Moku, F., Morou, B., Mucina,
739 L., Mugisha, S., Mwavu, E., Rutherford, M., Sanou, P., Syampungani, S., Tomor, B., Vall, A., Vande Weghe,
740 J., Wangui, E., & Waruingi, L. (2013). *A New Map of Standardized Terrestrial Ecosystems of Africa*.
741 Washington, DC: Association of American Geographers.
742
743 Seghieri, J., Do, F.C., Devineau, J.-L., Fournier, A., others, 2012. Phenology of woody species along the
744 climatic gradient in west tropical Africa. *Phenology and climate change*. Intech Open Access Publisher 143–
745 178.
746
747 Sexton, J.O., Song, X.-P., Feng, M., Noojipady, P., Anand, A., Huang, C., Kim, D.-H., Collins, K.M.,
748 Channan, S., DiMiceli, C., Townshend, J.R., 2013. Global, 30-m resolution continuous fields of tree cover:
749 Landsat-based rescaling of MODIS vegetation continuous fields with lidar-based estimates of error.
750 *International Journal of Digital Earth* 6, 427–448. doi:10.1080/17538947.2013.786146
751
752 Spiekermann, R., Brandt, M., Samimi, C., 2015. Woody vegetation and land cover changes in the Sahel of
753 Mali (1967–2011). *International Journal of Applied Earth Observation and Geoinformation* 34, 113–121.
754 doi:10.1016/j.jag.2014.08.007
755
756 Sterling, S.J., Orr, B., 2014. Patterns of Tree Distribution within Small Communities of the Sudanian
757 Savanna-Sahel. *Land* 3, 1284–1292. doi:10.3390/land3041284
758

759 Townshend, J.R.G., M. Carroll, C. Dimiceli, R. Sohlberg M. Hansen, and R. DeFries., 2011. Vegetation
760 Continuous Fields MOD44B, 2001 Percent Tree Cover, Collection 5, University of Maryland, College Park,
761 Maryland, 2001.

762

763 Tracol, Y., Mougín, E., Hiernaux, P., Jarlan, L., 2006. Testing a sahelian grassland functioning model against
764 herbage mass measurements. *Ecological Modelling* 193, 437–446. doi:10.1016/j.ecolmodel.2005.08.033

765

766 Verger, A., Baret , F., & Weiss, M. (2008). Performances of neural networks for deriving LAI estimates from
767 existing CYCLOPES and MODIS products. *Remote Sensing of Environment*, 112, 2789-2803

768

769 Vintrou, E., Bégué, A., Baron, C., Saad, A., Lo Seen, D., Traoré, S.B., 2014. A Comparative Study on
770 Satellite- and Model-Based Crop Phenology in West Africa. *Remote Sensing* 6, 1367–1389.
771 doi:10.3390/rs6021367

772

773 Vries, F.W.T.P. de, Djitéye, M.A., 1982. La Productivité des pâturages sahéliens: une étude des sols, des
774 végétations et de l'exploitation de cette ressource naturelle. Centre for Agricultural Publishing and
775 Documentation.

776

777 Wagenseil, H., Samimi, C., 2007. Woody Vegetation Cover in Namibian Savannas: A Modelling Approach
778 Based on Remote Sensing (Die Gehölzdichte in den Savannen Namibias: eine fernerkundungsgestützte
779 Modellierung). *Erdkunde* 61, 325–334.

780

781 Weiss, M., Baret , F., Garrigues, S., Lacaze, R., & Bicheron, P. (2007). LAI, fAPAR and fCover CYCLOPES
782 global products derived from VEGETATION. part 2: Validation and comparison with MODIS Collection 4
783 products. *Remote Sensing of Environment*, 110, 317-331

784

785 Yang, W., Huang, D., Bin Tan, Stroeve, J.C., Shabanov, N.V., Knyazikhin, Y., Nemani, R.R., Myneni, R.B.,

786 2006. Analysis of leaf area index and fraction of PAR absorbed by vegetation products from the terra
787 MODIS sensor: 2000-2005. IEEE Transactions on Geoscience and Remote Sensing 44, 1829–1842.
788 doi:10.1109/TGRS.2006.871214

789

790 Zandler, H., Brenning, A., Samimi, C., 2015. Quantifying dwarf shrub biomass in an arid environment:
791 comparing empirical methods in a high dimensional setting. Remote Sensing of Environment 158, 140–155.
792 doi:10.1016/j.rse.2014.11.007

793

794

795 **Figure captions:**

796

797 *Figure 1: Conceptual approach of this study exemplified for VGT FAPAR*

798

799 *Figure 2: Overview of the Sahel zone and location of the 43 ground monitoring sites covering Senegal (west) and the*
800 *Gourma region in Mali. The Sahel delineation is based on annual average precipitation (African Rainfall Climatology*
801 *Version 2 1983–2013).*

802

803 *Figure 3: Seasonal distribution of woody leaf mass depending on the phenological type, modeled within the STEP*
804 *primary production simulation model (Mougin et al., 1995). The months of the wet season during which herbaceous*
805 *grow are highlighted in a shaded box. Illustrations of typical herbaceous growing curves can be found in Mougin et al.,*
806 *(2014).*

807

808 *Figure 4: Annual VGT FAPAR cycle of pixels with sparse and moderately dense woody cover. The two ground sites*
809 *(named C2L4 and C3L5) have contrasting values regarding woody cover, herb biomass and woody leaf biomass. All*
810 *values are averaged over 1999-2013. Biomass data are taken from Brandt et al. (2015). For abbreviations, see Table 1.*
811 *Whereas SINT represents the herbaceous layer, DSINT is proposed to reflect the woody layer.*

812

813 *Figure 5: Accuracy assessment, prediction and metric importance (a) for SPOT VGT and (b) for MODIS. The predicted*
814 *(multiple regression model) and cross-validation predicted values (using 4 subsamples to predict points not used to*

815 *establish the model) are plotted against corrected in situ data. CvRMSE is given in % woody cover. (c) Relative*
816 *importance of the variables used to predict corrected woody cover with 95% bootstrap confidence intervals for SPOT*
817 *VGT and (d) for MODIS. LMG method is used (Grömping, 2007) and metrics are normalized to sum 100%. For*
818 *abbreviations, see Table 1. (e) Uncorrected in situ data is plotted against predicted data after adjusting to the mean*
819 *foliage density (only VGT is shown). (f) Compares in situ data woody cover with MOD44B tree cover.*

820

821 *Figure 6: (a) Means of pixel values for woody cover by mean rainfall zones (Fig. 2) as derived from VGT, MODIS*
822 *FAPAR, or from the MOD44B product. (b) VGT and MODIS woody cover over the Sahel (plot uses a sample of 3% of*
823 *the cells) showing that pre-classified barren land in MODIS has woody cover up to 40% in VGT, preventing a higher*
824 *correlation. (c) Temporal FAPAR profiles of 4 ground sites showing (1) that the impact of uncorrected woody*
825 *cover/corrected woody cover (%) on the rainy season metrics is of minor importance and (2) the systematic gap*
826 *between MODIS and VGT, with MODIS overestimating the dry season FAPAR especially in sparsely vegetated areas.*

827

828 *Figure 7: Extrapolated woody cover maps derived from VGT (a) and MODIS (b) FAPAR as well as the global tree cover*
829 *product MOD44B (c). (d+e) show zooms to Senegal and Gourma (Mali) using VGT map (the squares in (a)). Masked*
830 *wetlands are displayed gray.*